

On-chip generation of indistinguishable photons using cavity quantum-electrodynamics

Kai Müller,^{1,*} Armand Rundquist,¹ Kevin A. Fischer,¹ Tomas Sarmiento,¹ Konstantinos G. Lagoudakis,¹ Yousif A. Kelaita,¹ Carlos Sánchez Muñoz,² Elena del Valle,² Fabrice P. Laussy,² and Jelena Vučković¹

¹*E. L. Ginzton Laboratory, Stanford University, Stanford, California 94305, USA*

²*Departamento de Física Teórica de la Materia Condensada, Universidad Autónoma de Madrid, 28049 Madrid, Spain*

(Dated: March 22, 2022)

The on-chip generation of non-classical states of light is a key requirement for future optical quantum hardware. In solid-state cavity quantum electrodynamics (QED), such non-classical light can be generated from self-assembled quantum dots (QDs) strongly coupled to photonic crystal cavities. Their anharmonic strong light-matter interaction results in large optical nonlinearities at the single photon level, where the admission of a single photon into the cavity may enhance (photon-tunnelling) or diminish (photon-blockade) the probability for a second photon to enter the cavity. Here, we demonstrate that detuning the cavity and QD resonances enables the generation of high-fidelity non-classical light from strongly coupled systems. For specific detunings we show that not only the purity but also the probability of single photon generation increases significantly, making almost-perfect single photon generation by photon-blockade possible with current state-of-the-art samples. Finally, we show that photon-blockade under fully resonant excitation is a promising candidate for the generation of indistinguishable single photons due to a short cavity lifetime that suppresses phonon dephasing.

Due to their strong interaction with light and ease of integration into optoelectronic devices, self-assembled quantum dots (QDs) are promising candidates for quantum light sources. High-fidelity single photon generation from QDs for off-chip applications has been demonstrated under both non-resonant¹ and resonant^{2–4} excitation. Some of these experiments have employed micropillar cavities⁵, etched⁶ or epitaxially grown photonic nanowires⁷ for enhanced light off-chip extraction efficiency. On the other hand, photonic crystal cavities provide a promising on-chip route toward optoelectronic integration of QDs due to the established set of associated integrated waveguide and detector structures^{8,9}. Such structures will be able to exploit strong light-matter coupling with QDs for the generation of a variety of on-chip non-classical light states by various quantum-electrodynamical methods, and recent exotic proposals have even explored the possibility of releasing energy exclusively in bundles of n -photons¹⁰. The phenomena of photon-tunnelling and photon-blockade in strongly

coupled systems have been experimentally demonstrated both for the case of the QD on resonance^{11–13} and near resonance¹⁴ with the cavity (and likewise, only for resonant atom-cavity system¹⁵). However, in the case of large detuning these effects have only been investigated theoretically, leading to the hypothesis that such detuned systems could be used to improve the quality of generated nonclassical states of light¹⁶.

In this paper, we demonstrate the feasibility of performing photon-blockade at significant detuning, and indeed the importance of doing so for high-fidelity operations. We show that by detuning the QD and cavity resonances while operating in the photon-blockade regime, the second-order autocorrelation function ($g^2(0)$) of the light transmitted through the cavity decreases from $g^2(0) = 0.9 \pm 0.05$ to $g^2(0) = 0.45 \pm 0.05$. Simulations of the second- and third-order autocorrelation functions for our system are in excellent agreement with the measurements, and they reveal that not only does the quality of the single photon stream increase, but that the absolute probability of obtaining a single photon increases by a factor of ~ 2 . Furthermore, we show that the values we obtain for $g^2(0)$ are only limited by the system parameters (QD-cavity field coupling strength g and cavity field decay rate κ), and that almost-perfect single photon emission is within reach for current state-of-the-art samples for specific cavity and QD detunings. To investigate the indistinguishability of single photons generated by photon blockade, we perform two photon interference measurements^{17,18} and obtain a visibility of 0.6; in our case, this value is shown to be mainly limited by $g^2(0)$. In general, however, single photons created by photon blockade exhibit a very high indistinguishability due to a short cavity lifetime that suppresses phonon dephasing and a fully resonant excitation condition that prevents temporal excitation jitter.

The sample investigated is schematically illustrated in figure 1a and consists of a layer of low density InAs QDs grown by molecular beam epitaxy and embedded in a photonic crystal L3 cavity¹⁹. The energy structure of a QD strongly coupled to a cavity is well described by the Jaynes-Cummings (JC) Hamiltonian

$$H = \omega_a a^\dagger a + (\omega_a + \Delta) \sigma^\dagger \sigma + g(a^\dagger \sigma + a \sigma^\dagger) \quad (1)$$

where ω_a denotes the frequency of the cavity, a the annihilation operator associated with the cavity mode, σ

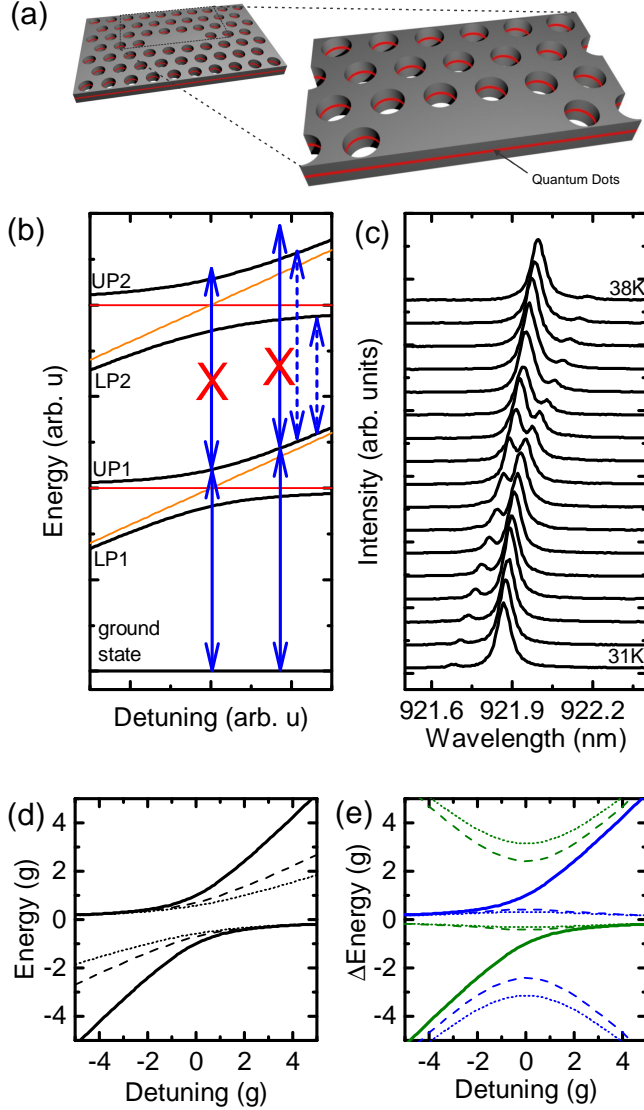


FIG. 1. (a) Schematic illustration of self-assembled quantum dots embedded in a photonic crystal cavity. (b) Schematic illustration of the Jaynes-Cummings ladder obtained from equation 1 that describes the energetic structure of a strongly coupled system. (c) Cross-polarised reflectivity spectrum of the coupled quantum dot-cavity system obtained by tuning the QD through the cavity resonance under temperature tuning. An anticrossing of the peaks clearly demonstrates the strong coupling. (d) Photon energies for exciting the n -th rung of the Jaynes-Cummings ladder in an n -photon process for the first, second and third rung as solid, dashed and dotted lines, respectively. (e) Transient energies for climbing the Jaynes-Cummings-ladder rung by rung for the first, second and third rung as solid, dashed and dotted lines, respectively. Transitions from upper and lower polaritons are colour coded in blue and green, respectively. In panels (d) and (e) the energy of the bare cavity was subtracted from all transitions for better comparability.

the lowering operator of the quantum emitter, Δ the

detuning between quantum emitter and cavity, and g the emitter-cavity field coupling strength. The resulting eigenenergies, the Jaynes-Cummings-ladder dressed states, are schematically illustrated in figure 1b. For n photons in the cavity the energy is $n\omega_a$, as depicted in red, and the energy of the quantum emitter depicted in orange varies with a detuning parameter (x-axis). Due to the coupling, the resulting energy eigenstates are the anticrossing polariton branches (solid lines in figure 1b) labelled LP_n and UP_n , for the lower and upper branches, respectively, with n being the index of the rung (i.e., the photon number in the cavity). At resonance, the splitting of the anticrossing branches is given by $2g\sqrt{n}$. We note here that while this manuscript explicitly discusses the case of a quantum dot in a photonic crystal cavity, the same physics holds for a large number of system such as those formed by atoms^{20,21} or superconducting circuits²².

For QDs, the anticrossing that results from the coupling to a cavity can be nicely studied in optical spectroscopy experiments, where the QD and cavity detuning is controlled by the lattice temperature^{23,24}. The result of such a measurement is presented in figure 1c, which shows the transmission through the cavity measured in a cross-polarised reflectivity configuration²⁵ in the temperature range $T = 31 - 38$ K. A clear anticrossing provides evidence of strong coherent coupling between quantum dot and cavity. A fit (not shown here) reveals a coupling strength of $g/2\pi = 10.9$ GHz and a cavity field decay rate $\kappa/2\pi = 10.0$ GHz.

Due to the unequal energy spacing (anharmonicity) of the Jaynes-Cummings ladder, transmission of a laser through the cavity affects the beam's photon statistics and introduces strong photon correlations^{11,14}. This is schematically illustrated by the solid blue arrows in figure 1b; if the laser is tuned into resonance with one of the polariton branches of the first rung, it cannot excite the system to the second rung due to the ladder anharmonicity. Therefore, in this regime the transmitted beam consists of a series of single photons and hence is called the photon-blockade regime. However, the fidelity of this process is inherently limited by the transition linewidth, given by the cavity field κ and quantum emitter γ decay rates. In particular, due to final state broadening and the shorter lifetime of higher rungs, transitions to higher rungs have larger linewidths, further reducing the probability of generating single photons.

It is important to note that although all photon-blockade experiments reported so far have been performed near the case of $\Delta = 0$, this configuration results in the lowest possible fidelity of single photon emission. We consider two cases to support this conclusion: the excitation of a higher rung in a multi-photon process and the excitation of the second rung following excitation of the first rung. In order to investigate both cases in detail, we plot the energies for an n -photon excitation of the n -th rung in figure 1d and the transient energies from one rung to the next in figure 1e. Figure 1d shows the energies for n -photon excitation of the first, second and

third rung as solid, dashed and dotted lines, respectively. Clearly, at zero detuning the energies for exciting the first and higher rungs are close together, and their separation strongly increases for the upper (lower) polariton branch for positive (negative) detunings of the quantum emitter. This demonstrates that for a laser in resonance with the first rung the probability of n -photon excitation of higher rungs decreases with increased detuning. Similar scenarios can be found for subsequent climbs up the ladder, as presented in figure 1e, which shows the transition energies from the ground state to the first rung, the first to the second rung and the second to the third rung as solid, dashed and dotted lines, respectively. Transitions from an upper (lower) polariton branch to higher rungs are colour coded in blue (green). As examples, the transition from the ground state to UP1 and the subsequent transitions from UP1 to LP2 and UP2 are illustrated in figure 1b as solid and dashed blue arrows, respectively (using the same color and solid or dashed coding as in figure 1e). Near resonance the first and second transitions are close in energy but their separation strongly increases with the detuning of the quantum emitter (c.f. blue arrows in figure 1b). The close proximity of the first rung (solid lines) to the outer higher order transitions for large detunings does not reduce single photon emission character, since these transitions occur from the other polariton branch as can be seen from the different colours. Therefore, a detuning between quantum emitter and cavity is also expected to improve the fidelity of single photon generation under photon blockade for subsequent rung excitation. Furthermore, detuning also affects the linewidths of the states in such a way that the linewidth of a polariton branch that evolves towards the bare QD (bare cavity) transition decreases (increases). This further reduces the overlap of transitions involving different rungs of the JC ladder and increases the fidelity of photon-blockade (for details see supplemental material).

To quantify the quantum character of light the second-order autocorrelation function²⁶

$$g^2(0) = \frac{\langle a^\dagger a^\dagger a a \rangle}{\langle a^\dagger a \rangle^2} \quad (2)$$

is a commonly used quantity, which results in a $g^2(0)$ of 1 for a coherent source and 0 for a perfect stream of single photons. To test our expectation that the fidelity of single-photon generation under photon-blockade can be improved by detuning the QD and cavity resonances, we measured $g^2(0)$ from the output correlations of a laser beam transmitted through the cavity. The result of these experiments is presented in the left part of figure 2 that shows $g^2(0)$ as a function of the laser detuning for seven different QD and cavity detunings. The position of the bare cavity, bare QD and polariton branches is indicated by red, orange and black vertical lines, respectively. The data were recorded under pulsed excitation with $t_p = 30$ ps long pulses, derived from a 3 ps mode-locked Ti:sapphire laser using frequency filter-

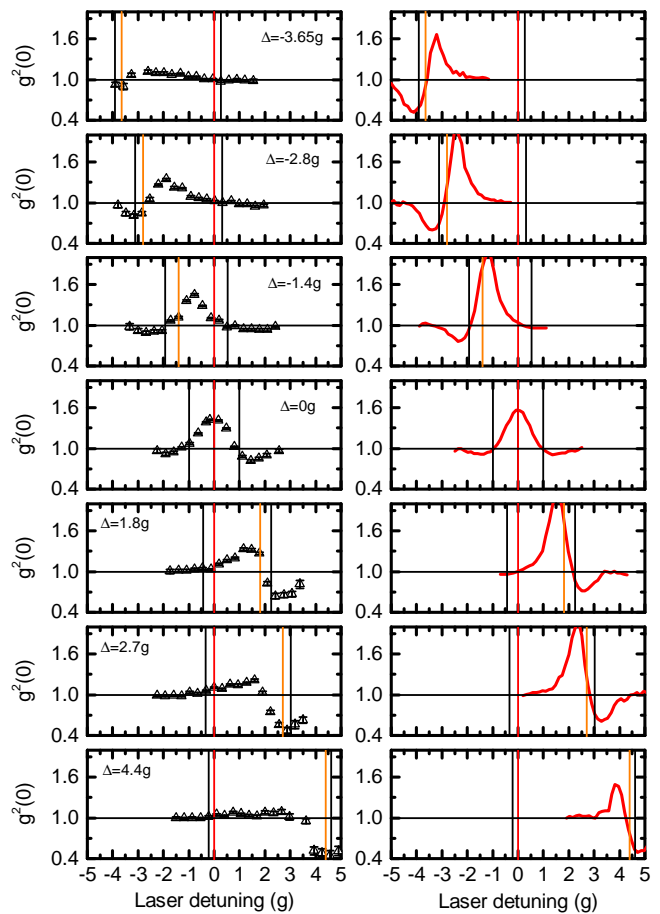


FIG. 2. $g^2(0)$ as function of the laser detuning for a set of different QD-cavity detunings: (left) experiment and (right) simulation. With increased detuning the depth of the anti-bunching is more pronounced. The positions of the bare cavity, bare QD and first rung dressed states branches are indicated by red, orange and black vertical lines, respectively.

ing. This pulse duration was chosen as a compromise between frequency resolution and avoiding re-excitation of the system. In the case of the tuned system (detuning $\Delta = 0$), the form of $g^2(0)$ is symmetric with photon tunnelling generating a maximum of $g^2(0) = 1.45 \pm 0.05$ in the centre, and photon-blockade generating a minimum dip of $g^2(0) = 0.85 \pm 0.05$ ($g^2(0) = 0.92 \pm 0.05$) at the laser detuning of $1.5g$ ($-1.5g$). Small asymmetries of the curve result from drift in the QD and cavity detuning over the time scale of our measurements, asymmetries in the spectral shape of the laser pulse, and wavelength dependence of the cross-polarised laser suppression. When detuning the QD, the maximum of $g^2(0)$ shifts such that it stays between the polariton branches before it disappears for detunings greater than $\sim 4g$. The dip of $g^2(0)$ both moves with and shifts toward the polariton branch that is closer to the bare QD transition. Most strikingly, the depth of the dip increases and reaches a value as low as $g^2(0) = 0.45 \pm 0.05$ for the detunings of $\Delta = 2.7g$ and

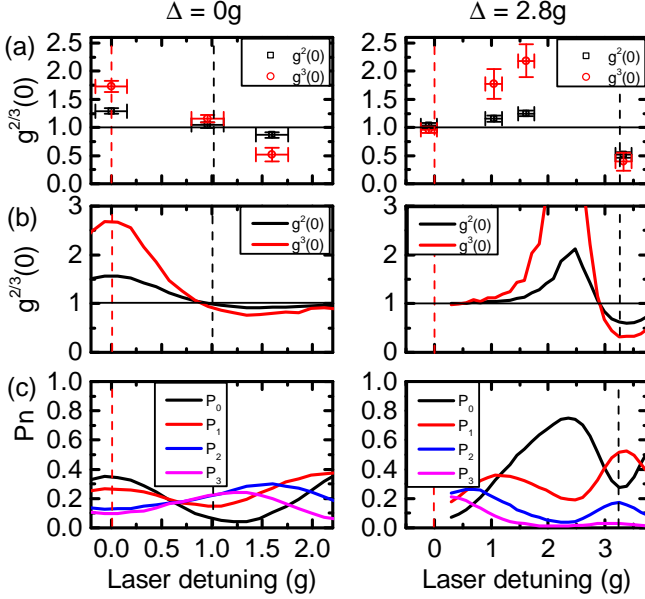


FIG. 3. (a) Measured second- and third-order autocorrelation functions as a function of the laser detuning for a QD detuning of $\Delta_{QD} = 0$ (left) and $\Delta_{QD} = 2.8g$ (right). (b) Simulation of the second and third order correlation functions for the experimental conditions presented in (a). (c) Simulated probabilities for having $n = 0 - 4$ photons in the output of a pulse transmitted through the cavity. Clearly, for a detuning of $\Delta_{QD} = 2.8g$ (right) P_1 (red) exhibits a pronounced peak.

$\Delta = 4.4g$. This value is lower than 0.5, the threshold for evidence of emission from a single quantum emitter, and lower than $g^2(0)$ measured in any prior photon blockade experiments.

To support our findings, we performed quantum optical simulations using a quantum trajectory method (see methods section). The results of these simulations are presented on the right side of figure 2, which shows the simulated values of $g^2(0)$ for the same parameters as the corresponding experimental data presented on the left side of figure 2. Overall, the simulations are in excellent qualitative agreement with the measurements and also quantitatively resemble the values measured in the photon-blockade regime. Only small differences exist: the measured maximum values of $g^2(0)$ are slightly lower than the simulated ones. This can be explained by blinking of the quantum emitter¹⁴, which was not included in the simulations.

To further investigate the single photon character of the light transmitted through the cavity we performed measurements of the third-order autocorrelation function $g^3(0) = \frac{\langle a^\dagger a^\dagger a^\dagger a a a \rangle}{\langle a^\dagger a \rangle^3}$, as higher-order autocorrelations are necessary to characterise the multi-photon nature of non-classical light²⁷. The result of these measurements are presented in figure 3a, which shows $g^2(0)$ and $g^3(0)$ as a function of the laser detuning for the case of QD-cavity detuning of $\Delta = 0$ (left) and $\Delta = 2.8g$ (right). Clearly,

$g^3(0)$ shows the same qualitative shape as $g^2(0)$ but with stronger non-classical values. Simulations of these autocorrelations are presented in figure 3b and show good agreement with the measurements. In particular, for the photon-blockade regime the values of $g^3(0)$ are lower than those of $g^2(0)$, indicating that $g^2(0)$ is mainly limited by two photon events and not higher photon events.

Since the agreement with the measured autocorrelation functions is very good, we can rely on the simulations to explicitly access quantities only within reach of the theory, such as the probabilities P_n of transmitting n photons per excitation pulse through the cavity. These probabilities are presented in figure 3c for $n = 0 - 3$ under the same conditions as the data presented in figure 3a and 3b. Interestingly, we find that in the case of zero QD and cavity detuning (figure 3c left), we see significant contributions of one, two and three photon events for all laser detunings. In fact, the probability for two photon events (blue) actually dominates over the probability for single photons (red) in the case of the best photon blockade. In strong contrast, for a QD-cavity detuning of $\Delta = 2.8g$ (figure 3c right) and operation in the photon-blockade regime, single photon events (red) strongly dominate over two photon events (blue) and the probability for three photon events (purple) becomes negligible. Most strikingly, in the detuned case, not only does the quality of the single photon stream increase, but the absolute probability of finding a single photon in the transmitted laser pulse increases by a factor of ~ 2 . This further corroborates the importance of detuning in obtaining high-fidelity single photon streams under photon blockade.

Next, we discuss the potential for single photon generation using detuned photon-blockade given already achievable system parameters. Improvements in the spatial alignment of the QD and cavity field have enabled the coupling strength to reach values up to $g/2\pi = 40$ GHz²⁸. Additionally, recent nanofabrication improvements have allowed for experimental GaAs photonic crystal cavity loss rates as low as $\kappa/2\pi = 4.0$ GHz²⁹. When using these parameters in our simulations for a detuned system we obtain $g^2(0) = 0.1$ in the photon-blockade regime, and an absolute probability of over 90% for single photon emission, demonstrating that nearly perfect single photon streams generated by photon-blockade are within reach. As discussed earlier, high-fidelity generation of single photons with QDs in cavities has been demonstrated under a large set of experimental conditions, without exploiting cavity QED effects. However, the generation of single photons by photon-blockade has a number of advantages over other techniques. First, the cavity lifetime is at least one order of magnitude smaller than the bare QD lifetime, resulting in an order of magnitude improvement in the maximum single photon generation rate. Second, this configuration could be used to generate a high-indistinguishability single photon stream, as discussed below. In addition, the use of high quality photonic crystal cavities promises a method of on-chip rout-

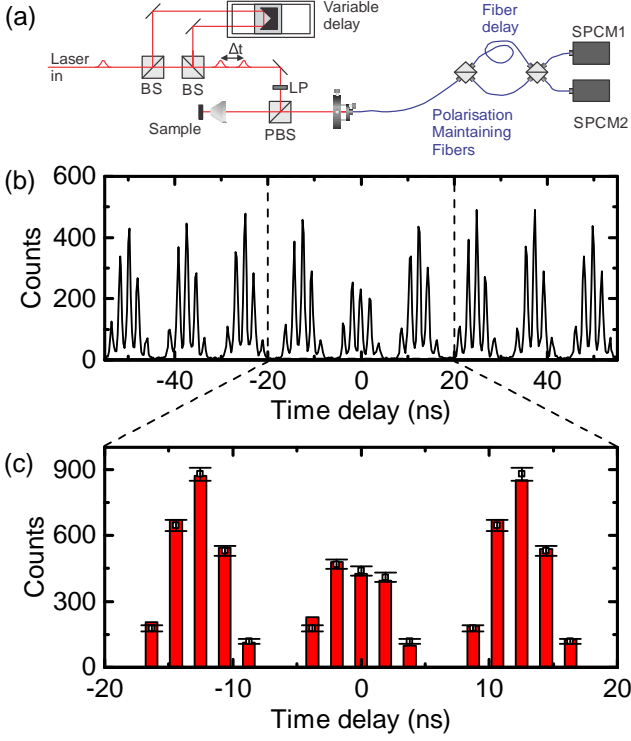


FIG. 4. (a) Schematic illustration of the setup used to measure photon indistinguishability. (b) Measured correlation function of the transmitted photon stream showing five peaks per excitation pulse pair, corresponding to various combinations of paths of the 2 photons from the pair through the HOM interferometer. At 0 time delay the amplitude of the three centre peaks is reduced. (c) Amplitudes around zero delay obtained from binning the data presented in (b) with a temporal width of 512 ps about the centre of each peak. Fits to the data are presented as black data points and reveal $g^2(0) = 0.5$ and an indistinguishability of $V = 0.6$

ing of the photons by coupling them to photonic crystal waveguides (with high efficiency)³⁰.

Having shown that the on-chip generation of nearly perfect single photon streams is possible, we continue to investigate the indistinguishability of photons generated by photon-blockade. In general, the indistinguishability of single photons generated from QDs is limited by frequency jitter, timing jitter (in the case of non-resonant excitation) and phonon dephasing during the radiative lifetime¹⁸. Therefore, single photons created by photon-blockade should show a high indistinguishability, as the transmission through a cavity is a fully resonant process and the short cavity lifetime largely suppresses interaction with phonons. To experimentally investigate the indistinguishability of single photons generated by photon-blockade, we performed two photon interference measurements as schematically illustrated in figure 4a. From the spectrally filtered picosecond laser with repetition rate 80 MHz, we created a pulse train consisting of two pulses of identical power and tunable time delay (figure 4a left).

These pulses are transmitted through the cavity using a cross-polarised geometry (figure 4a bottom-left) and the transmitted light is coupled into a polarisation maintaining fibre (figure 4a centre). The light then passes through a Hong-Ou-Mandel (HOM) interferometer based on non-polarising beamsplitters coupled to polarisation maintaining fibres, whose output ports are coupled to two single photon detectors (figure 4a right). We note that one of the fibres between the two beamsplitters is longer, with a length difference that corresponds to a time difference of $\Delta T_1 = 1.9$ ns. When the variable delay is set to ΔT_1 , the first pulse can interfere with the second pulse only if the first and second pulses take the long and short path, respectively. The interference is then measured as a series of correlations between the two single photon detectors.

The result of a typical measurement recorded in the photon-blockade regime is presented in figure 4b for a QD-cavity detuning of $\Delta = 3g$. A pattern of five peaks is observed every 12.5 ns with the time difference of ΔT_1 between the peaks. As a result of the two photon interference and the single photon character of the transmitted pulses, the three centre peaks around zero time delay are suppressed¹⁸. The asymmetry of the five peaks is a result of the imperfect splitting ratios of the nominally 50 : 50 beam splitters. To quantitatively analyse the data we bin the counts in a time window of 512 ps about the peaks. The result of this binning for a time delay in the range -20 to 20 ns is presented as red bars in figure 4c. Taking the measured ratio $R_1 : T_1 = 50 : 50$ for the first beam-splitter, the amplitudes of the five peaks (A_{1-5}) are given by

$$A_1 = A \cdot R^2 \quad (3)$$

$$A_2 = A \cdot (2TR + 2R^2g^2(0)) \quad (4)$$

$$A_3 = A \cdot (4RTg^2(0) + (R^2 + T^2(1 - 2V))) \quad (5)$$

$$A_4 = A \cdot (2TR + 2T^2g^2(0)) \quad (6)$$

$$A_5 = A \cdot T^2 \quad (7)$$

where R and T are the reflectivity and transmittance of the second beamsplitter, V the indistinguishability of two subsequent pulses and A the amplitude. The amplitudes for peaks away from zero time delay are obtained by using $g^2(0) = 1$ and $V = 0$. A fit to the data using the measured values $R : T = 55 : 45$ is presented as black datapoints in figure 4c and produces excellent agreement using the parameters $g^2(0) = 0.5 \pm 0.05$ and $V = 0.6 \pm 0.05$. We note here that in the case of an imperfect single photon source, such as our system, V does not denote the indistinguishability of two single photons but rather the indistinguishability of two subsequent pulses transmitted through the cavity. Therefore, in our case with $g^2(0) = 0.5$ the obtained value of $V = 0.6$ is limited by $g^2(0)$, making photon-blockade from detuned cavity QD system a promising approach for high-fidelity generation of indistinguishable photons.

In summary, we have demonstrated that QD-cavity detuning is a key ingredient for high-fidelity generation of

non-classical light from strongly coupled cavity QD systems. We have shown that detuning strongly reduces the spectral overlap with higher rungs of the Jaynes-Cummings-ladder and hence greatly improves the generation of single photons by photon-blockade. We have presented quantum-optical simulations that are in excellent agreement with our measurements and show that almost-perfect single photon generation under photon blockade is possible with current state-of-the-art samples. Finally, we have shown that single photons generated by photon blockade have a high indistinguishability due to suppression of phonon dephasing and excitation temporal jitter. The successful experimental demonstration of photon-blockade in the detuned light-matter configuration demonstrates the feasibility of operating cavity QED in such an extreme regime and paves the way for a wealth of other quantum light sources, even operating beyond the single-photon level¹⁰.

ACKNOWLEDGEMENTS

We gratefully acknowledge financial support from the Air Force Office of Scientific Research, MURI Center for Multifunctional light-matter interfaces based on atoms and solids and support from the Army Research Office (grant number W911NF1310309). KM acknowledges financial support from the Alexander von Humboldt Foundation. KGL acknowledges financial support from the Swiss National Science Foundation. KAF acknowledges support through Lu Stanford Graduate Fellowship. YAK acknowledges support through Stanford Graduate Fellowship and National Defense Science and Engineering Graduate Fellowship.

METHODS

Sample fabrication

The MBE grown structure consists of a ~ 900 nm thick $Al_{0.8}Ga_{0.2}As$ sacrificial layer followed by a 145 nm thick GaAs layer that contains a single layer of InAs QDs. Our growth conditions result in a typical QD density of $60 - 80 \mu\text{m}^{-2}$. The photonic crystals were fabricated using 100 keV e-beam lithography with ZEP resist, followed by reactive ion etching and HF removal of the sacrificial layer. The photonic crystal lattice constant was $a = 246$ nm and the hole radius $r \approx 60$ nm. The cavity fabricated is a linear three-hole defect (L3) cavity. To improve the cavity quality factor, holes adjacent to the cavity were shifted^{31,32}.

Optical spectroscopy

All optical measurements were performed with a liquid helium flow cryostat at temperatures in the range 10 – 40 K. For excitation and detection a microscope objective with a numeric aperture of $NA = 0.75$ was

used. Cross-polarised measurements were performed using a polarising beam splitter. To further enhance the extinction ratio, additional thin film linear polarisers were placed in the excitation/detection pathways and a single mode fibre was used to spatially filter the detection signal. Furthermore, two waveplates were placed between the beamsplitter and microscope objective: a half-wave plate to rotate the polarisation relative to the cavity and a quarter-wave plate to correct for birefringence of the optics and sample itself.

Autocorrelation measurements

Second-order autocorrelation measurements were performed using a Hanbury Brown and Twiss (HBT) setup consisting of one fibre beamsplitter and two single photon avalanche diodes. The detected photons were correlated with a PicoHarp300 time counting module. Third order autocorrelation measurements were performed using a generalised HBT setup consisting of three fibre beamsplitters that result in a balanced splitting of the signal into four channels and four single photon avalanche diodes. In the generalised setup, the detected photons were correlated using a sensL four channel multi-stop time-tagging counting module. Two photon interference measurements were performed with the same detectors and electronics as the second order correlation measurements but with a Hong-Ou-Mandel interferometer replacing the single beamsplitter, as discussed in the main text.

Simulations

Details on the simulations of correlations and the relation between measured and simulated values can be found in the supplemental material. In short, our simulations are based in the rotating wave approximation, and the dynamics are simulated with the quantum jump method using the Quantum Optics Toolbox in Python (QuTiP)³³, which generates quantum trajectories that are solutions for our system's associated stochastic Schrödinger equation. Monitoring collapse events of the cavity field over many trajectories generates the expected photocount distribution. From this distribution, we directly compute the normalised second order factorial moment in order to simulate our experimentally measured $g^2(0) = \frac{\langle n(n-1) \rangle}{\langle n \rangle^2}$.

AUTHOR CONTRIBUTIONS

KM, AR and KGL performed the experiments. TS performed the MBE growth of the QD structure. AR and TS fabricated the photonic crystal device. KAF performed the simulations. YAK, CS, EdV and FPL provided expertise and analysis tools. JV supervised the entire project. All authors contributed to discussions and writing the manuscript.

-
- * kaim@stanford.edu
- ¹ C. Santori, M. Pelton, G. Solomon, Y. Dale, and Y. Yamamoto, *Physical Review Letters* **86**, 1502 (2001).
 - ² C. Matthiesen, A. N. Vamivakas, and M. Atatüre, *Phys. Rev. Lett.* **108**, 093602 (2012).
 - ³ Y.-M. He, Y. He, Y.-J. Wei, D. Wu, M. Atatüre, C. Schneider, S. Hofling, M. Kamp, C.-Y. Lu, and J.-W. Pan, *Nat Nano* **8**, 213 (2013).
 - ⁴ S. Ates, S. M. Ulrich, S. Reitzenstein, A. Löffler, A. Forchel, and P. Michler, *Phys. Rev. Lett.* **103**, 167402 (2009).
 - ⁵ O. Gazzano, S. Michaelis de Vasconcellos, C. Arnold, A. Nowak, E. Galopin, I. Sagnes, L. Lanco, A. Lemaître, and P. Senellart, *Nature Communications* , 1425 (2013).
 - ⁶ J. Claudon, J. Bleuse, N. S. Malik, M. Bazin, P. Jaffrennou, N. Gregersen, C. Sauvan, P. Lalanne, and J.-M. Gérard, *Nature Photonics* **4**, 174 (2010).
 - ⁷ M. E. Reimer, G. Bulgarini, N. Akopian, M. Hocevar, M. B. Bavinck, M. A. Verheijen, E. P. A. M. Bakkers, L. P. Kouwenhoven, and V. Zwiller, *Nature Communications* **3**, 737 (2012).
 - ⁸ J. P. Sprengers, A. Gaggero, D. Sahin, S. Jahanmirinejad, G. Frucci, F. Mattioli, R. Leoni, J. Beetz, M. Lermer, M. Kamp, S. Höfling, R. Sanjines, and A. Fiore, *Applied Physics Letters* **99**, 181110+ (2011).
 - ⁹ G. Reithmaier, S. Lichtmannecker, T. Reichert, P. Hasch, K. Muller, M. Bichler, R. Gross, and J. J. Finley, *Sci. Rep.* **3** (2013), 10.1038/srep01901.
 - ¹⁰ C. S. Muñoz, E. del Valle, A. G. Tudela, K. Müller, S. Lichtmannecker, M. Kaniber, C. Tejedor, J. J. Finley, and F. P. Laussy, *Nature Photonics* **8**, 550 (2014).
 - ¹¹ A. Faraon, I. Fushman, D. Englund, N. Stoltz, P. Petroff, and J. Vuckovic, *Nature Physics* **4**, 859 (2008).
 - ¹² A. Faraon, A. Majumdar, and J. Vučković, *Phys. Rev. A* **81**, 033838 (2010).
 - ¹³ A. Majumdar, M. Bajcsy, and J. Vučković, *Phys. Rev. A* **85**, 041801 (2012).
 - ¹⁴ A. Reinhard, T. Volz, M. Winger, A. Badolato, K. J. Hennessy, E. L. Hu, and A. Imamoglu, *Nature Photonics* , 9396 (2011).
 - ¹⁵ K. M. Birnbaum, A. Boca, R. Miller, A. D. Boozer, T. E. Northup, and H. J. Kimble, *Nature* **436**, 87 (2005).
 - ¹⁶ F. P. Laussy, E. del Valle, M. Schrapp, A. Laucht, and J. J. Finley, *Journal of Nanophotonics* **6**, 061803 (2012).
 - ¹⁷ C. K. Hong, Z. Y. Ou, and L. Mandel, *Phys. Rev. Lett.* **59**, 2044 (1987).
 - ¹⁸ C. Santori, D. Fattal, J. Vučković, G. S. Solomon, and Y. Yamamoto, *Nature* **419**, 594 (2002).
 - ¹⁹ Y. Akahane, T. Asano, B.-S. Song, and S. Noda, *Nature* **425**, 944 (2003).
 - ²⁰ M. Brune, F. Schmidt-Kaler, A. Maali, J. Dreyer, E. Hagley, J. M. Raimond, and S. Haroche, *Phys. Rev. Lett.* **76**, 1800 (1996).
 - ²¹ I. Schuster, A. Kubanek, A. Fuhrmanek, T. Puppe, P. W. H. Pinkse, K. Murr, and G. Rempe, *Nature Physics* **4**, 382 (2008).
 - ²² J. M. Fink, M. Goppl, M. Baur, R. Bianchetti, P. J. Leek, A. Blais, and A. Wallraff, *Nature* **454**, 315 (2008).
 - ²³ J. P. Reithmaier, G. Sek, A. Löffler, C. Hofmann, S. Kuhn, S. Reitzenstein, L. V. Keldysh, V. D. Kulakovskii, T. L. Reinecke, and A. Forchel, *Nature* **432**, 197 (2004).
 - ²⁴ K. Hennessy, A. Badolato, M. Winger, D. Gerace, M. Atatüre, S. Gulde, S. Fält, E. L. Hu, and A. Imamoglu, *Nature* **445**, 896 (2007).
 - ²⁵ D. Englund, A. Faraon, I. Fushman, N. Stoltz, P. Petroff, and J. Vuckovic, *Nature* **450**, 857 (2007).
 - ²⁶ R. J. Glauber, *Phys. Rev.* **130**, 2529 (1963).
 - ²⁷ A. Rundquist, M. Bajcsy, A. Majumdar, T. Sarmiento, K. Fischer, K. G. Lagoudakis, S. Buckley, A. Y. Piggott, and J. Vuckovic, *arXiv:1307.3601* (2014).
 - ²⁸ D. Takamiya, Y. Ota, R. Ohta, H. Takagi, N. Kumagai, S. Ishida, S. Iwamoto, and Y. Arakawa, *2013 Conference on Lasers and Electro-Optics Pacific Rim*, 2013 Conference on Lasers and Electro-Optics Pacific Rim , MI2 (2013).
 - ²⁹ Y. Ota, S. Iwamoto, N. Kumagai, and Y. Arakawa, *Phys. Rev. Lett.* **107**, 233602 (2011).
 - ³⁰ A. Faraon, I. Fushman, D. Englund, N. Stoltz, P. Petroff, and J. Vuckovic, *Opt. Express* **16**, 12154 (2008).
 - ³¹ Y. Akahane, T. Asano, B.-S. Song, and S. Noda, *Opt. Express* **13**, 1202 (2005).
 - ³² M. Minkov and V. Savona, *Scientific Reports* **4** (2014), 10.1038/srep05124.
 - ³³ J. Johansson, P. Nation, and F. Nori, *Computer Physics Communications* **184**, 1234 (2013).
 - ³⁴ R. Loudon, *The Quantum Theory of Light* (Oxford Science Publications, 2000).

SUPPLEMENTAL MATERIAL

Relation between $g^2(0)$ and correlation measurements

The expression $g^2(0) = \frac{\langle a^\dagger a^\dagger aa \rangle}{\langle a^\dagger a \rangle^2}$ is commonly used to describe the second-order field autocorrelation of a given light beam. Following Loudon³⁴, we first discuss the validity of this expression as used in this context and mention that it is somewhat incomplete. A semiclassical treatment of photodetection defines the measured degree of second-order coherence at zero time delay as $g^2(0) \equiv \frac{\langle m(m-1) \rangle}{\langle m \rangle^2}$, which is the normalized second order factorial moment of the time integrated photocount distribution $P_m(T)$. In analogy to the classical integrated mean intensity, the quantum mechanical operator

$$\hat{M}(T) = \int_0^T dt b^\dagger(t)b(t) \quad (8)$$

represents the total photon number arriving at an ideal detector over the time interval $t \in [0, T]$, such that $\langle m \rangle = \langle \hat{M}(T) \rangle$. Here, $b(t)$ is the instantaneous field mode operator describing the field flux - it is important to note its distinction with the cavity field mode operator $a(t)$: $b(t)$ describes a field flux while $a(t)$ describes a field. Comparing our semiclassical definition of $g^2(0)$ to the quantum mechanical operator $\hat{M}(T)$, we have

$$g^2(0) = \frac{\langle \hat{M}(T)(\hat{M}(T) - 1) \rangle}{\langle \hat{M}(T) \rangle^2} = \frac{\langle : \hat{M}(T)^2 : \rangle}{\langle \hat{M}(T) \rangle^2} \quad (9)$$

where $\langle : \hat{M}^2(T) : \rangle$ denotes the quantum mechanical expectation value of the normally ordered second moment of the photon number operator. Writing out this expression explicitly

$$g^2(0) = \frac{\int_0^T \int_0^T dt dt' \langle b^\dagger(t)b^\dagger(t')b(t')b(t) \rangle}{\left(\int_0^T dt \langle b^\dagger(t)b(t) \rangle \right)^2} \quad (10)$$

and substituting the un-normalized correlation moments for the expectation values, we arrive at

$$g^2(0) = \frac{\int_0^T \int_0^T dt dt' G_{bb}^2(t, t')}{\langle m \rangle^2} \quad (11)$$

Therefore, the measured $g^2(0)$ actually represents a quantity other than that which $\frac{\langle a^\dagger a^\dagger aa \rangle}{\langle a^\dagger a \rangle^2}$ would suggest. Instead of representing the correlation between two photon number (Fock) states, states that incidentally do not exist in free space, $g^2(0)$ represents the sum of all field flux correlations $G_{bb}^2(t, t')$ over the detection time. In other words, $\frac{\langle a^\dagger a^\dagger aa \rangle}{\langle a^\dagger a \rangle^2}$ operates only on states which are well defined in a cavity whereas the correlation measurements are performed on fluxes. However, input-output theory provides a direct connection between

the internal and external mode operators such that measuring zero delay flux correlations is equivalent to calculating $\frac{\int_0^T \int_0^T dt dt' \langle a^\dagger(t)a^\dagger(t')a(t')a(t) \rangle}{\left(\int_0^T dt \langle a^\dagger(t)a(t) \rangle \right)^2}$ inside the cavity.

Details on the simulations of $g^2(0)$ and P_n

Assuming the rotating wave approximation (RWA) and a rotating reference frame relative to the laser field (frequency ω_l), the Jaynes-Cummings Hamiltonian describing interaction of our strongly coupled system with a laser pulse takes the form

$$H = \Delta_{QD}\sigma_+\sigma_- + \Delta_a a^\dagger a + g(a^\dagger\sigma_- + a\sigma_+) + \mathcal{E}(t)(a + a^\dagger) \quad (12)$$

where σ_\pm are the dipole operators, a is the cavity mode operator, and $\mathcal{E}(t)$ the slowly vary field-cavity coupling amplitude. The self-energies and their shifts in the rotating frame are defined by $\Delta_{QD} = \omega_{QD} - \omega_l$ and $\Delta_a = \omega_a - \omega_l$, where ω_{QD} and ω_a are the atomic and cavity energies, respectively. We take the laser pulse as a Gaussian, well described by $\mathcal{E}(t) = \mathcal{E}_0 \exp(-\frac{t^2}{2\tau_p^2})$, where $\tau_p = 30$ ps is the pulse parameter. In simulations, we find that \mathcal{E}_0 results in correlations that closely match the observed experimental data. Additionally, we assume that the cavity decay, κ , dominates the loss dynamics because the quantum dot lifetime is almost two orders of magnitude larger than the cavity lifetime.

The simulations presented in this paper are performed using the Quantum Optics Toolbox in Python (QuTiP)³³. To simulate the second order correlation function two different approaches are used: the quantum regression theorem and the quantum jump method. Application of the quantum regression theorem to a problem of the form

$$\langle A(t)B(t+\tau)C(t+\tau)D(t) \rangle \quad (13)$$

yields the following result

$$\langle A(t)B(t+\tau)C(t+\tau)D(t) \rangle = \text{Tr}_{\text{sys}}\{BC\Lambda(t, t+\tau)\} \quad (14)$$

where $\Lambda(t, t+\tau)$ is governed by the following evolution equation

$$\partial_r \Lambda(t, t+\tau) = \mathcal{L}(t+\tau)\Lambda(t, t+\tau) \quad (15)$$

subject to the initial condition

$$\Lambda(t, t) = D\rho(t)A \quad (16)$$

Since equation 10 has the same form as equation 13, the implementation of the quantum regression theorem for the calculation of $g^2(0)$ is straight-forward.

In the quantum jump method, quantum trajectories that are solutions for our system's associated stochastic Schrödinger equation are calculated. Monitoring collapse events of the cavity field over many trajectories generates the expected photocount distribution that would be

measured by an ideal, infinite bandwidth detector placed directly at the cavity output. From this distribution, we directly compute the normalised second order factorial moment in order to simulate our experimentally measured $g^2(0) = \frac{\langle n(n-1) \rangle}{\langle n \rangle^2}$.

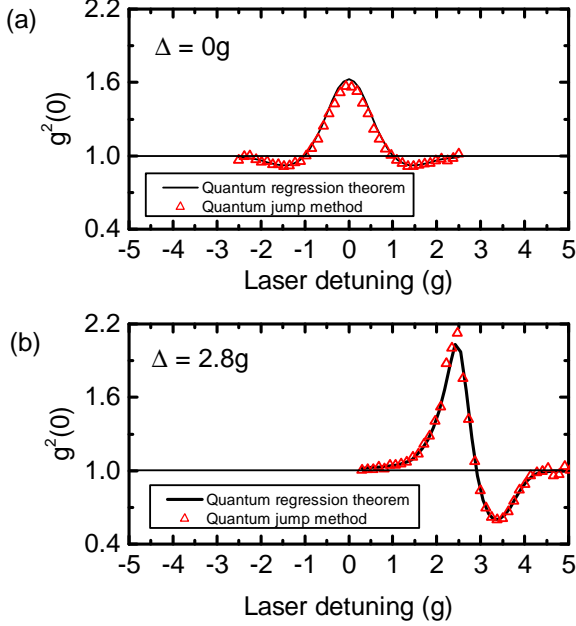


FIG. 5. Simulated $g^2(0)$ obtained using the quantum regression theorem (solid lines) and quantum jump method (red data points) for a QD-cavity detuning of (a) $\Delta = 0$ and (b) $\Delta = 2.8g$

While using the quantum regression theorem results in a faster simulation of $g^2(0)$, the quantum jump method additionally provides explicitly the probabilities for n photons per pulse being transmitted through the cavity. To validate that the quantum jump method works well in our case and that we have simulated a sufficiently large

number of quantum trajectories, we present in figure 5 simulated values of $g^2(0)$ as a function of the laser detuning for two different cavity - QD detunings (c.f. figure 2 in the main manuscript), as obtained from the quantum regression theorem and quantum jump method (black solid lines and red datapoints, respectively). Clearly, both methods produce excellent agreement.

Finally, we note that because the correlation functions describing photon statistics are robust to loss and our detectors have finite detection probability paired with low photon coincidence probability, the experimentally measured and normalized coincidences from the HBT setup should very closely match this simulated values.

LINEWIDTHS OF DETUNED SYSTEMS

Using the Liouville equation, dissipation can be introduced into the JC Hamiltonian, resulting in complex energies of the JC system that read¹⁶:

$$E_{\pm}^n = n\omega_a - \frac{\Delta}{2} - i\frac{(2n-1)\kappa + \gamma}{4} \pm \sqrt{(\sqrt{n}g)^2 + \left(\frac{\Delta}{2} - i\frac{\kappa - \gamma}{4}\right)^2} \quad (17)$$

where E_{\pm}^n corresponds to the n th rung of the system. The real part of E_{\pm}^n yields the energies of the states whereas the imaginary part yields their linewidths. Interestingly, all four parameters κ , γ , Δ and g contribute to the polariton splittings and linewidths. Most strikingly, for the case of QDs and photonic crystal cavities with $\kappa \gg \gamma$, the linewidth of a given polariton branch closer to the bare QD (bare cavity) under detuning is smaller (larger) than at resonance. This is particularly important for photon-blockade phenomena that rely on the absence of an energetic overlap between: transitions from the crystal ground state to the first rung and transitions from the first rung to higher rungs. Therefore, detuning the cavity and QD not only increases the energy difference between transitions involving different rungs but also decreases the linewidth of the polariton branches closer to the bare QD transition, thus further enhancing the fidelity of photon-blockade.